

Journal of Materials Chemistry A

Accepted Manuscript



This is an *Accepted Manuscript*, which has been through the Royal Society of Chemistry peer review process and has been accepted for publication.

Accepted Manuscripts are published online shortly after acceptance, before technical editing, formatting and proof reading. Using this free service, authors can make their results available to the community, in citable form, before we publish the edited article. We will replace this *Accepted Manuscript* with the edited and formatted *Advance Article* as soon as it is available.

You can find more information about *Accepted Manuscripts* in the [Information for Authors](#).

Please note that technical editing may introduce minor changes to the text and/or graphics, which may alter content. The journal's standard [Terms & Conditions](#) and the [Ethical guidelines](#) still apply. In no event shall the Royal Society of Chemistry be held responsible for any errors or omissions in this *Accepted Manuscript* or any consequences arising from the use of any information it contains.

Effects of surface-modified silica nanoparticles attached graphene oxide using isocyanate-terminated flexible polymer chains on the mechanical properties of epoxy composites

Tongwu Jiang^a, Tapas Kuila^b, Nam Hoon Kim^{a*}, Joong Hee Lee^{a,c,*}

3-aminopropyltriethoxysilane (APTES) surface-modified silica nanoparticles were attached to graphene oxide (GO) using isocyanate group-terminated flexible chains in order to synthesize silica nanoparticles attached GO (SATPGO). The SATPGOs synthesized at various compositions were used as reinforcing fillers to prepare epoxy composites. Fourier transform infrared (FT-IR) spectroscopy and X-ray photoelectron spectroscopy analyses confirmed the surface modification of silica nanoparticles after surface grafting with the silane coupling agent, 1,2,4-benzenetricarboxylic anhydride, followed by cross-linking of the surface-modified silica nanoparticles to GO. X-ray diffraction analysis confirmed the attachment of silica nanoparticles to fully exfoliated GO sheets. Transmission electron microscopy images revealed that the silica nanoparticles were introduced uniformly onto the GO sheets. The mechanical properties (impact and tensile properties) of the SATPGO/epoxy composites were dramatically enhanced with the addition of small amount of SATPGO. The storage modulus of the SATPGO filled epoxy composites was higher than that of pure epoxy. The impact strength of SATPGO (0.5 wt. %)/epoxy composite improved by 154% at room temperature and by 92% at 77 K without any sacrifice of the tensile properties. Moreover, the tensile strength and modulus of the epoxy resin improved with SATPGO loading. The improvements of the thermal stability and mechanical properties were attributed to the synergistic effects of the silica nanoparticles, flexible polymer chains, and GO ternary system.

1. Introduction

Epoxy has a variety of technological and potential applications in aerospace, electrical, electronics, land and marine transportation industries due to its superior insulation behavior, good mechanical stability, ease of handling, low cost, excellent dimensional stability, good adhesion, and chemical resistance compared to other thermosetting resins.^{1,2} However, the main drawback of neat epoxy is its inherently brittle nature, which makes it notch sensitive and leads to a poor composite toughness. The poor crack resistance of epoxy at room temperature (RT) is more pronounced at cryogenic temperatures (CT), which restricts the use of neat epoxy in advanced cryogenic engineering applications. Therefore, it is of great importance to improve the fracture toughness and strength of epoxy at cryogenic temperatures for cryogenic applications. Many works have been devoted to achieve this goal and over the years, several approaches have been reported. Flexible chain diamines,³ thermoplastic poly(ethersulfone) (PSF),⁴ polyetherimide (PEI),⁵ polyphenylene (PPE),⁶ poly(ethylene terephthalate) (PET),⁷ phenoxy,⁸ polycarbonate (PC),⁹ silica nanoparticles,¹⁰ exfoliated montmorillonite (MMT),¹¹ hyperbranched polymers,¹² polyurethane,¹³ and n-butyl glycidyl ether¹⁴ have all been proposed as cryogenic toughening agents for epoxy. However, the use of thermoplastic toughening agents is often problematic due to the high processing temperature during melt mixing, as it causes degradation and the formation of defective composites. The removal of entrapped solvent from thermoplastic toughening agents after solution mixing is also a significant issue. Organic/inorganic composites are frequently employed to overcome these limitations. A representative organic/inorganic system is an epoxy/silica blend. Advancements in nanotechnology as well as processing techniques have resulted in the commercial availability of nanometer scale silica particles as reinforcing fillers for polymer composites. The use of nano-silica

decreases the shrinkage in curing and thermal expansion coefficient. In contrast, the thermal conductivity and mechanical properties may improve under cryogenic conditions. However, at higher filler loadings mechanical properties of the composite may deteriorate due to the agglomeration of nano-silica particles.

Recently, the novel two-dimensional material, graphene oxide (GO), has triggered numerous fundamental and technological studies on polymer composites¹⁵ because GO possesses unique properties including a high aspect ratio, surface area, elastic modulus, fracture strength, and thermal conductivity.^{16,17} GO and surface modified GO were used as a building block for new polymer composites to obtain high performance composite materials.¹⁸⁻²³ The use of GO as reinforcing filler is advantageous in terms of mechanical property improvement due to the presence of various oxygen functional groups leading to strong interfacial interaction between GO and polymer.^{24,25} However, it is thermally unstable and can readily undergo exothermic disproportionation reactions under mild heating conditions leading to the loss of thermal stability.²⁶ Moreover, -NH₂ functional groups of the hardener molecules may directly react with the epoxide functionalities of GO resulting incomplete crosslinking of the epoxy resin. In order to overcome these shortcomings, GO and silica nanoparticles can potentially be cross-linked using flexible organic molecules. Thus, a unique approach involves the simultaneous functionalization and cross-linking of GO and silica in order to improve their dispersion in a polymer matrix.^{27,28} GO consists of intact graphitic regions interspersed with sp³ hybridized carbons containing hydroxyl and epoxide functional groups on the top and bottom surfaces of each sheet. Isocyanate-modified GO can be exfoliated in polar, aprotic solvents to yield GO derivatives. In addition, the use of isocyanate-containing surface modifying agents with cyano, keto, and azidosulfonyl functionalities would allow for further modification of the surface properties and chemistry of modified GO.²⁹

In this study, a new strategy to prepare cross-linked GO with modified silica is proposed. Herein, the surface of silica nanoparticles was modified with 3-aminopropyltriethoxysilane (APTES) and carboxyl group-terminated silica was obtained via grafting of 1, 2, 4-benzenetricarboxylic anhydride (TMA) to the silanized silica. Isocyanate-terminated flexible chains were synthesized by the reaction of toluene diisocyanate (TDI) with different molecular weight poly(ethylene glycol) (PEG) chains. APTES-modified silica nanoparticles attached GO (SATPGO) via isocyanate group-terminated flexible chains were prepared from carboxyl group-terminated silica nanoparticles and GO. The effects of SATPGOs on the dispersion in epoxy and mechanical properties of the composites were investigated.

2. Experimental

2.1. Materials

Concentrated sulfuric acid (98%), hydrochloric acid, and hydrogen peroxide were purchased from Samchun Pure Chemical Co. Ltd, Korea. Potassium permanganate purchased from Junsei Chemical Co. Ltd, Japan was used as the oxidizing agent. Dibutyltindilaurate (DBTDL), 1,2,4-benzenetricarboxylic anhydride (TMA), sodium bicarbonate, p-toluenesulfonic acid (PTSA), and poly(ethylene glycol) (PEG 200, 400, and 600) were purchased from Alfa Aesar, USA. Toluene diisocyanate (TDI) was purchased from Tokyo Chemical Industry Co. Ltd, Japan. The diglycidyl ether of bisphenol A (DGEBA) epoxy YD-128 was purchased from Kukdo Chemical Co. Ltd, Korea, and had an epoxide equivalent weight of 172.8 g/equiv. JEFFAMINE® D-230 amine, a polyether diamine curing agent, was supplied by Kukdo Chemical Co. Ltd, Korea. Expanded graphite was purchased from Sigma-Aldrich, USA and used as received. The silane coupling agent, 3-aminopropyltriethoxysilane, and silica foam (particle size of 7 nm) were purchased from Sigma-Aldrich, USA.

2.2. Preparation of GO, APTES-modified SiO₂, and carboxyl group-terminated SiO₂

GO was prepared according to the modified Hummer's method, as reported previously.³⁰ For silane modification of SiO₂, approximately 0.5 mL of APTES was dissolved in 150 mL of ethanol under stirring for 10 min. Approximately 2 g of silica foam was dispersed into the solution by ultrasonication for 30 min. The ternary mixture was stirred and heated to 60 °C for 8 h to complete the silanization reaction. Silica particles were separated from the mixture and washed several times with a mixture of ethanol and DI water to remove excess coupling agent. The obtained product was designated as SA. The as-prepared SA was dispersed into THF via ultrasonication to obtain an oozing, blue, and transparent liquid. TMA was then added to the suspension and the mixture was stirred for 8 h at room temperature. Excess TMA was removed by washing with DI water via centrifugation. The obtained product was designated as SAT.

2.3. Synthesis of SATPGO

SATPGO was synthesized from PEG and TDI in the presence of DBTDL. PEG was heated under vacuum at 120 °C for 120 min to remove moisture. A stoichiometric amount of dried PEG was

added drop-wise to TDI for 15-30 min under a dry nitrogen atmosphere. DBTDL (0.1 wt%) was used as a catalyst for the reaction. The reaction mixture was refluxed at 80 °C for 2 h to prepare the isocyanate-terminated flexible chain cross-linker. SAT (1.5 g) was ultrasonicated in anhydrous THF (50 ml) for 30 min and then, the isocyanate cross-linker and GO were introduced into a three-necked flask under stirring. A catalytic amount of PTSA was added to the mixture and the mixture was heated to 70 °C for 5 h. The final product was washed with sodium bicarbonate solution to remove the catalyst, followed by washing several times with DI water. The final product was then freeze-dried. The details of the synthesis procedure are shown in scheme 1. The SATPGOs prepared with various molecular weights of PEG₂₀₀, PEG₄₀₀, and PEG₆₀₀, where the subscripts refer to the molecular weight of PEG, were designated as SATPGO₁, SATPGO₂, and SATPGO₃, respectively. The yield of each SATPGO was approximately 80%.

2.4. Fabrication of SATPGO-filled epoxy composites

A stoichiometric amount of SATPGOs (SATPGO₁, SATPGO₂, or SATPGO₃) was ground to a fine powder using a mortar and pestle. The fine powder was dispersed into acetone via water bath ultrasonication for 1 h. DGEBA monomer was heated to 60 °C in a drying oven to reduce its viscosity. An acetone dispersion of SATPGO was then added to the epoxy at 80 °C under vigorous stirring. After complete evaporation of the acetone, the mixture was further vacuum degassed for 1 h. After cooling to room temperature, the D-230 (30 wt.% of epoxy) curing agent was added and the above mixture was mixed thoroughly in a vacuum mixer for 5 min. Finally, the gas-less, homogeneous mixture was poured into a silicon mold, cured at 80 °C for 2 h, and then post-cured at 125 °C for 3 h.

2.5. Characterization

Fourier-transform infrared (FT-IR) spectra of expanded graphite, SiO₂, SA, SAT, GO, and SATPGO were recorded on a Thermo Fisher Scientific spectrometer (Thermo Scientific, USA) using the attenuated total reflectance (ATR) technique. The spectra were scanned at RT over the frequency range of 4,000-500 cm⁻¹. The X-ray diffraction (XRD) patterns of expanded graphite, SiO₂, GO, and SATPGO were measured on a D8 ADVANCE X-ray diffractometer (Bruker, Germany) using Cu-K α radiation (λ =0.154 nm) at a generator voltage of 40 kV and a current of 50 mA. The scanning range was fixed at 1-60° with a scanning rate of 2° min⁻¹. Thermogravimetric analysis (TGA) was conducted from 30 °C to 800 °C at a heating rate of 10 °C min⁻¹ under a nitrogen and air atmosphere using a Q50 thermogravimetric analyzer (TA Instruments, USA). The calorimetric measurement of the composites were also performed using a Q50 differential scanning calorimeter (DSC) (TA Instruments, USA) equipped with a thermal analysis data station, operating at a heating rate of 10 °C min⁻¹ under a constant flow of nitrogen of 50 mL min⁻¹ from the ambient temperature to 300 °C. The glass transition temperature (T_g) was taken as the midpoint of the capacity change. Dynamic mechanical analysis (DMA) was performed using a Q 800 DMA (TA instruments, USA) in the fixed frequency mode at 1 Hz with an amplitude of 0.40 mm, in the

temperature range of 30-150 °C, at a heating rate of 2 °C min⁻¹. Rectangular specimens with dimensions of 60 × 10 × 3 mm³ were used for DMA test. X-ray photoelectron spectroscopy (XPS) of GO and SATPGO was performed with monochromatic Al-K α (1,486.71 eV) radiation at the KBSI Jeonju Center using an AXIS-NOVA analyzer (Kratos Analytical Ltd, UK). Powdered samples of GO and SATPGO were used for the XPS analysis. Atomic force microscopy (AFM) was performed using a Digital Instrument Nanoscope IIIa scanning probe microscope operating under tapping mode. AFM samples were prepared by spin-coating the dispersions of GO and modified GO onto freshly cleaved silicon substrates at 3000 rpm.

The fracture surfaces of the specimens after impact testing were examined on a JSM-6701F (JEOL, Japan) field emission scanning electron microscope (FE-SEM). Prior to examination, the fracture surfaces were sputter-coated with gold to improve the conductivity. Elemental analysis was also performed with the same equipment. Transmission electron microscopy (TEM) images were recorded using a JEM-2200FS (JEOL, Japan). For this analysis, GO was dispersed into water (~0.2 mg mL⁻¹) and sonicated for 30 min. The suspension was dropped onto a 400-mesh lacey carbon copper grid. Similarly, SATPGO (~0.2 mg mL⁻¹) was dispersed into THF by ultrasonication for 30 min, followed by drop casting onto a 400-mesh lacey carbon copper grid. The samples were dried at RT prior to the TEM analysis. The TEM samples of the SATPGO-filled epoxy composites were prepared by the microtome method. About 70-80 nm thick slices of the composite film were cut using a microtome (Leica Ultracut, Germany) using a diamond knife and were transferred onto 400-mesh copper grids (Ted Pella, Inc., USA) at room temperature.

Dumbbell-shaped tensile specimens were prepared according to the ASTM D 638-10 standard and tested using a mechanical testing system (MTS, LandmarkTM, USA) under a 10 kN load cell with a cross-head speed of 2 mm min⁻¹. The dimensions of the working section of the tensile specimen were 63.5 mm (length) × 9.53 mm (width) × 3.2 mm (thickness). Six specimens were evaluated for each test group. The cryogenic tensile testing was performed in a cryogenic chamber. The impact strength was measured using a Zwick/Roell HIT25P Izod impact tester (Zwick/Roell, Germany) according to ASTM D-256. The dimensions of the specimens for the impact test were 64 mm (length) × 12.7 mm (width) × 6.35 mm (thickness). The specimens for the cryogenic impact testing were immersed in liquid nitrogen for over 5 min to reach a temperature of 77 K before evaluation. Impact testing was performed immediately after mounting the specimen and each test was completed in a couple of seconds. Single edge notched bending (SENB) tests were performed to measure the mode I fracture toughness of pure epoxy and the composites by determining the critical stress intensity factor, K_{IC} , following the ASTM D 5045-99 method. The specimen dimensions were 150 mm × 20 mm × 10 mm. A prefab slot notch with a depth of ~4 mm was created by a fretsaw and a sharp pre-crack was initiated with a razor blade in the notch. All tests were carried out at 20 °C using a universal testing

machine (ULM-T2, R&B Co., Korea) with a constant crosshead speed of 10 mm min⁻¹. The load-deflection curves of all of the specimens obtained from the SENB testing were linear until breaking, especially when the stress near the crack tip was small. The fracture toughness, K_{IC} , was calculated using linear elastic fracture mechanics as follows:³¹

$$K_{IC} = \frac{SP_C}{BW^{3/2}} f(x) \quad (1)$$

$$f(x) = \frac{3x^{1/2}[1.99 - x(1-x)(2.15 - 3.93x + 2.7x^2)]}{2(1+2x)(1-x)^{3/2}} \quad (2)$$

$$x = \frac{a_0}{W} \quad (3)$$

where S is the span length, P_C is the maximum load, B and W are the thickness and width of the specimen, respectively, and a_0 is the pre-crack length of the specimen.

3. Results and Discussion

3.1. FT-IR spectroscopy analysis

FT-IR spectroscopy was employed to investigate the functionalization of GO, as shown in Fig. 1. The characteristic band intensities of GO corresponding to C=O carbonyl stretching at 1,723 cm⁻¹, O-H deformation at 1,404 cm⁻¹, C-OH stretching at 1,226 cm⁻¹, and epoxy and alkoxy stretching vibrations at 1,053, respectively, were significantly decreased in the modified GO (SATPGO₁, SATPGO₂ and SATPGO₃), suggesting partial reduction of GO during the surface modification process.³²⁻³⁴ The broad band at 3,400 cm⁻¹ and intense peak at 1,621 cm⁻¹ were assigned to the vibrations of adsorbed water molecules and skeletal vibrations of non-oxidized carbon domains, respectively. In comparison to the pristine silica, silane coupling agent-modified silica revealed characteristic stretching vibration peaks for Si-O-Si and Si-OH at 1,113 and 943 cm⁻¹, respectively. A Si-OH bending vibration peak appeared at 804 cm⁻¹. New peaks for SA (1,570 to 1,350 cm⁻¹) corresponding to N-H, C-H, and C-N stretching or bending vibrations of the APTES moieties were observed. These observations confirmed the silane modification of the SiO₂ nanoparticles. Upon treatment with isocyanate, the C=O stretching vibration of GO at 1,733 cm⁻¹ became obscured by the appearance of a stronger absorption band at 1,703 cm⁻¹. It may be attributed to the carbonyl stretching vibration of surface hydroxyl carbonate esters in SATPGO₁, SATPGO₂, and SATPGO₃. The new peak at 1,646 cm⁻¹ was assigned to the amide carbonyl stretching mode. The band at 1,543 cm⁻¹ was attributed to either amides or carbonate esters, corresponding to coupling of the C-N stretching vibration with the CHN deformation vibration. The contraction vibration peaks at 1,652 and 1,714 cm⁻¹ corresponding to -CO-NH- and -C=O groups, respectively, indicated that TMA was effectively grafted onto the surface of the silanized silica. Thus, the FT-IR analysis suggested partial reduction and surface modification of GO with silanized silica nanoparticles.

3.2. XRD analysis

Fig. 2 shows the XRD patterns of graphite, SiO₂, GO, and SATPGO₂. The interlayer distance of the precursor-expanded graphite was 0.34 nm, as indicated by the (002) peak near 26°. Upon oxidation, the interlayer spacing of GO increased to ~0.76 nm, indicating the presence of oxygen functional groups. The XRD pattern of SATPGO₂ displayed a broad band centered at 2θ = 22.2° suggesting the formation of a few layers of silanized silica functionalized GO sheets. It is expected that the existence of branched silica nanoparticles prevented the aggregation of functionalized GO sheets. The presence of surface modifiers might be helpful for the dispersion of the silica nanoparticles and GO in the epoxy matrix. The XRD pattern also confirmed the absence of any ordered crystalline structure. Moreover, there is no detectable peak in the small angle area, suggesting the formation of partially exfoliated GO sheets.

3.3. XPS analysis

XPS was utilized to further explore the chemical interactions between the cross-linked GO and silane-modified silica. Fig. 3 (a,b) show the XPS survey curves of GO and SATPGO₂. The high resolution scan spectra in the N1s, Si2p, O1s, and C1s regions are shown in Fig. 3(c-f). The survey spectrum of SATPGO₂ displays the existence of Si2p (95 and 110 eV), C1s (285 eV), O1s (533.2 eV) and N1s (400 and 407 eV) bands. The XPS elemental analysis indicated that SATPGO₂ was composed of silicon (9.19%), carbon (52.28%), oxygen (25.8%), and nitrogen (11.38%). The presence of Si and N in the SATPGO₂ might be originated from APTES and isocyanate, respectively. The C1s spectra GO (Fig. 3 (c)) showed different chemical environments including C-C/C=C, C-O, C-O-C and O-C=O at 284.2, 286.4, 288.3 and 289.4 eV, respectively. Similarly, the C1s XPS of SATPGO₂ showed four peaks corresponding to C-C/C=C, C-O, C-O-C and C=O at 284.5, 286.4, 288.2 and 287.4 eV, respectively. The disappearance of O-C=O peak suggested partial reduction of GO with silanized silica nanoparticles. Interestingly, the peak intensities of the oxygen functionalities decreased significantly in SATPGO₂, further confirming the partial reduction of GO. The appearance of two strong bands for Si2p at 102.2 and 103.8 eV indicated the formation of Si-C and Si-O-Si bonds, respectively. The deconvoluted N1s XPS of SATPGO₂ exhibited two peaks at 399.6 and 399.8 eV corresponding to C-N and -NH-C=O/-NH, respectively. All of these findings suggested the simultaneous surface modification of GO with silanized silica nanoparticles via isocyanate-terminated flexible chains and partial reduction of GO.

3.4. Morphological analysis

The TEM images of GO and SATPGO₂ revealed a large area GO sheet with wrinkles on the copper grid (Fig. 4 (a-c)). The TEM image of SATPGO₂ showed the presence of silica nanoparticles on the rGO sheets. The isocyanate-terminated flexible chain cross-linked APTES-modified silica nanoparticles were attached to the surface of GO. The rGO sheets with wrinkles are known to be a favorable configuration for providing strong interfacial interactions with a polar epoxy matrix. The HR-TEM image of SATPGO₂ shown in Fig. 4b confirmed the presence of modified silica nanoparticles on the surface of the as-prepared few layer-

functionalized rGO sheets. The selected area electron diffraction (SAED) pattern of SATPGO₂ (Fig. 5c) showed a six-fold symmetric pattern, indicating the crystalline structure of partially reduced GO. The appearance of unresolved diffraction spots in the SAED pattern of SATPGO₂ was attributed to isocyanate-terminated flexible chain cross-linked APTES-modified silica on the rGO sheets.

The SATPGO₂ and GO were characterized by AFM as shown in the supporting information (Fig. S1). The AFM images of SATPGO₂ exhibited little aggregated particles, indicating silica nanoparticles were wrapped around GO sheets as shown in Fig. S1 (a). The thickness of SATPGO₂ was in the range of 30-90 nm. However, the thickness of the pristine GO sheet was ~1.26 nm, indicating single layer of GO in Fig. S1 (b). In addition, single silica nanoparticles were not found in the scanned area of the mica substrate, confirming good attachment of silica particles on the surface of graphene with the flexible polymers.

The microstructure of the SATPGO₂ was investigated by FE-SEM analysis as shown in Fig. S2. The FE-SEM image of SATPGO₂ showed the light gray particles (Fig. S2 (a)), confirming the attachment of silica nanoparticles on the rGO sheets. Elemental mapping of Si using energy dispersive X-ray (EDX) analysis was carried out to confirm the existence of silica nanoparticles (blue particles) on the surface of GO sheets in Fig. S2 (b). This observation is in good agreement with the observation of TEM analysis confirming the decoration of rGO sheets with SiO₂ nanoparticles.

3.5 Raman spectra analysis

Raman spectroscopy was utilized to characterize GO and its derivatives. Fig. 5 shows the Raman spectra of GO, SATPGOs, and the SATPGOs/epoxy composites. The spectrum of GO showed two prominent peaks at ~1342 and 1595 cm⁻¹ corresponding to the D and G peaks, respectively. The G band is attributed to the vibration of sp² hybridized carbon, whereas the D mode corresponds to the sp³ hybridized carbon, defects associated with the vacancies and grain boundaries. It is interesting to note that the intensity ratios of the D to G bands (I_D/I_G) in SATPGOs increased as compared to that of the pristine GO. The attachment of silica nanoparticles on the surface of GO sheets led to an enhancement of the I_D/I_G ratios, as shown in Fig. 5. Ferrari *et al.* showed that both the G and 2D bands can be used to clearly identify graphene sheets up to the 5 layers. Bilayer sheets have a broader and symmetrical 2D peak, while graphene sheets with more than five layers or bulk graphite exhibit similar characteristics. It was previously reported that the G peak position of single layer graphene shifted to lower frequencies and the intensity of the 2D band decreased after the stacking of more graphene layers. The peak positions of the G bands of GO, SATPGOs, and SATPGOs/epoxy composites were centered at ~1,595 cm⁻¹. These results indicated that the SATPGOs had fewer layers as compared to the GO. Moreover, the SATPGOs and SATPGOs/epoxy composites exhibited a broader and symmetrical 2D peak in the 2,500-3,500 cm⁻¹ region, suggesting the formation of a few layers of functionalized GO. The Raman spectra results agreed well with the TEM observations. The XPS results indicated that most of the oxygen functional groups were

eliminated and sp^3 hybridized carbons were converted to sp^2 hybridized carbons due to the cross linking reaction. The single or few layer-modified GO sheets would be dispersed well in the epoxy, resulting in enhanced interfacial interactions between the SATPGO and epoxy and thus, enhanced mechanical properties.

3.6. TGA and DSC analysis

TGA was performed to investigate the thermal stability of SiO_2 , SA, SAT, GO, SATPGO₁, SATPGO₂, SATPGO₃, and their epoxy composites in a N_2 atmosphere (Fig. 6 (a)). GO showed a slight weight loss from RT to 150 °C and a significant loss from 150 to 200 °C caused by the decomposition of oxygen-containing functional groups.^{47,48} The weight of GO further decreased up to 800 °C due to the degradation of carbon backbone. Pristine silica showed a loss of hydroxyl groups in the range of 250-800 °C with a calculated weight loss of ~2.3%.⁴⁹ Similarly, the onset degradation of SA was initiated at 200 °C, suggesting the decomposition of the terminal amine groups of the silane coupling agent grafted on the surface of the silica. In contrast, the weight loss (~7.3%) in the second stage between 550-800 °C was attributed to the decomposition of Si-O-Si bonds and short alkyl branched chains. The weight loss of SAT showed a similar trend to that of SA and ~12.7% weight loss was recorded in the range of 550-800 °C. The degradation of SATPGO occurred in the range of 150-450 °C due to the thermal decomposition of isocyanate group-terminated PEG chains and carboxyl group-terminated short chains grafted onto the silica surface. The negligible weight loss between 450-800 °C was attributed to the decomposition of silane coupling agent-saturated alkyl chains near the surface of the silica and removal of more stable oxygen-containing groups.⁵⁰ The SATPGO curves exhibited similar trends to those obtained for SA and SAT. However, SATPGO₂ was more stable than SATPGO₁ and SATPGO₃. The TGA curves of neat epoxy and the SATPGO₁ (0.5 wt.%), SATPGO₂ (0.5 wt.%), and SATPGO₃ (0.5 wt%) filled epoxy composites are shown in Fig. 6(h-k). Neat epoxy and SATPGO/epoxy composites showed significant weight loss at ~350 °C due to the decomposition flexible cross-linker chains and short chains attached to the surface of silica. The enhanced thermal stability of the composites was due to the strong interfacial interactions between fillers and epoxy matrix. In addition, the interpenetrating networks of the flexible surface modifiers and epoxy chains might also played an important role in enhancing the thermal stability of the composites. The TGA curves performed in air atmosphere showed two decomposition stages as shown in Fig. 6 (b). The first stage was due to the thermal degradation of epoxy network and the second one was due to the oxidation process of the char moiety.⁵¹ The thermal stabilities of all the materials studied under N_2 and air atmosphere were compared in Table S1. Interestingly, thermal stability of the composites in air atmosphere is more stable than that at N_2 atmosphere. It may be attributed to the formation of protective charred layer of SiO_2 on the surface of the composite materials, disrupting the oxygen supply from the atmosphere to the specimen.^[52]

The DSC curves of pure epoxy and SATPGOs/epoxy composites were presented in Fig. S3. The pure epoxy had a glass transition temperature (T_g) of ~93.8 °C. In contrast, the SATPGOs (0.5 wt%)/epoxy composites exhibited higher T_g (93.8 - 96.2 °C) as

compared to the neat epoxy. It may be due to the presence of SATPGOs in the epoxy matrix, which restricted the molecular mobility of the polymer chains resulting the increase of T_g values. It is expected that the presence of SATPGOs in epoxy would affect the crosslinking density of the resin, which may also be responsible for the change of T_g .

3.7. Mechanical properties

Fig. 7 (a-c) show the effects of the SATPGO content on the tensile strengths, tensile modulus, and impact strength of the epoxy composites studied at RT and CT. Mechanical properties of the composites studied both at RT and CT were appreciably higher than that of epoxy matrix. Initially, the tensile and impact strengths increased with increasing filler content and demonstrated maximum values at a 0.5 wt.% of filler loadings. The addition of 0.5 wt.% of SATPGO₁, SATPGO₂, and SATPGO₃ resulted 119, 154, and 128% improvements of impact strength at RT as compared to pure epoxy. Similarly, the improvements of the tensile strength of the composites with the same contents were 14, 19, and 16%, respectively. The impact and tensile strengths of the composites at CT showed similar trends to those at RT. The improvement in impact strength of epoxy composites filled with 0.5 wt.% of SATPGO₁, SATPGO₂, and SATPGO₃ at CT were 67, 92, and 80%, respectively. The improvement in tensile strength at CT was recorded as 41, 49, and 45%, respectively. The improvement in impact strengths of the composites was attributed to the interfacial interactions between the fillers and epoxy.²⁴ The combination of crack trapping, bridging and blunting mechanism among the flexible chain surface modifiers, silica nanoparticles and GO might also played an important role in controlling the mechanical properties of the composites.⁵³ In addition, it is expected that the load is transferred from the matrix to filler causing higher stiffness of the composites. Interestingly, the impact strength at RT was higher than that at CT for neat epoxy and composites. In contrast, the tensile strength at CT was consistently higher than that at RT for the same content of SATPGOs. It may be attributed to the decreased molecular mobility of the epoxy matrix resulting brittle nature of the composites at CT.⁵⁴ Thus, the tensile strengths of the composites at CT were higher than those measured at RT. It is also interesting to note that the mechanical properties of the composites were changed with the variation of SATPGOs types. Among the studied SATPGOs, SATPGO₂/epoxy composites exhibited highest impact and tensile strengths. It may be attributed to the better compatibility of the medium molecular weight flexible polymer chain modified SiO_2 -GO with the epoxy matrix.

The tensile modulus of the composites at CT was also higher than that at RT. The improvements of the tensile modulus of the composites with 1.0 wt.% of SATPGO₁, SATPGO₂, and SATPGO₃ at CT were 20, 33, and 27%, respectively. These improvements were decreased to 17, 31, and 23% at RT. Unlike other toughening agents, SATPGO simultaneously enhanced the impact and tensile properties at RT and CT because of the complex structures of the rigid silica nanoparticles, flexible polymer cross-linker, and GO with a high aspect ratio. The stress-strain curves of neat epoxy and SATPGO/epoxy composites measured at two different temperatures (RT and CT) are shown in

supporting information (Fig. S4). It is evident that the tensile strength and failure strain are simultaneously enhanced both at RT and at CT by the introduction of SATPGOs. Moreover, the SATPGO/epoxy composites exhibited relatively ductile behavior compared to pure epoxy. The K_{IC} values of neat epoxy and the SATPGO/epoxy composites were measured at 25 °C, as shown in Fig. 8. The high cross-link density of neat epoxy resulted in brittleness and a low fracture toughness indicating poor energy absorption during fracture.²⁸ The fracture toughness increased with increasing SATPGO contents and reached a maximum value at 0.5 wt% loading. The addition of 0.5 wt.% SATPGO₁, SATPGO₂, and SATPGO₃ to the epoxy matrix resulted in enhancement of the critical stress intensity factor (K_{IC}) by ~ 77, 90, and 84%, respectively. The fracture toughness can be attributed to the stress field in the matrix, which depends on the elastic and dynamic moduli of the particles packing with a constant particle volume.⁵⁵ As the SATPGOs content increased, the inter-particle distance increased, leading to heterogeneity in the epoxy matrix due to the cross-linked flexible chains and interpenetration by epoxy molecules. Therefore, the heterogeneity and strong interactions appeared to strengthen and toughen the epoxy matrix, resulting in the higher strength and fracture toughness of the SATPGO/epoxy composites compared to neat epoxy. Moreover, the introduction of flexible chains between the silica particles and GO sheets led to the absorption of a higher fracture energy and reduced the brittle nature of the epoxy matrix.^{41,56}

DMA was performed to measure the storage modulus, loss modulus and damping behavior of the SATPGOs filled composites. The storage modulus and $\tan \delta$ of the pure epoxy and the composite are shown in Fig. 9. Evidently, the storage modulus of the composite was enhanced with the addition of SATPGOs as compared to that of the pure epoxy. The storage moduli of SATPGO₁, SATPGO₂, and SATPGO₃ filled epoxy composites at 30 °C were 2149, 2382 and 2295 MPa, respectively. These values were almost 3.6, 14.9 and 10.7% higher than that of the pure epoxy. The increase in storage modulus in the glassy region suggested strong interfacial bonding among the polar functional groups of rigid SATPGOs with epoxy matrix. It is also expected that the stress is transferred from the matrix to the rigid fillers resulting the increase in storage modulus of the SATPGOs filled epoxy composites.⁵⁷ Interestingly, SATPGO₂ filled composite showed highest storage modulus among the tested samples, indicating that PEG₄₀₀ is the most effective flexible polymer chain in the preparation of effective reinforcing filler. The $\tan \delta$ is a conversed value that represents a difference in temperature. The peak temperature at $\tan \delta_{max}$ of the SATPGO/epoxy composites was 1-3 °C higher as compared with the pure epoxy composites, showing the enhanced thermal property attributed to the introduced SATPGOs. It agreed well with the T_g value from the DSC curve.⁵⁸

3.8. Fracture surface analysis of the composites

The impact fracture surfaces of pure epoxy and SATPGOs/epoxy composites were analyzed by FE-SEM, as shown in Fig. 10(a-k). The FE-SEM images of neat epoxy (fractured at RT and CT) revealed that the cracks spread freely and regularly throughout

the entire surfaces. Moreover, the fracture surfaces were very smooth accounting poor impact resistance of neat epoxy at RT and CT. Interestingly, the CT-fractured surfaces were smoother, plainer, and glassier than at RT suggesting more brittle nature of epoxy at CT than that at RT.⁵⁹ The fracture surfaces of the RT-fractured composites (Fig. 10c, f, and i) became very rough with the incorporation of SATPGOs (0.5 wt%), suggesting improved impact strength of the composites. The fracture surfaces of the SATPGO₂/epoxy composite were coarser than the composites containing SATPGO₁ and SATPGO₃, indicating higher impact strength of the composites. The formation of interfacial shear zones in the composites was also very clear as compared to that of the neat epoxy.⁶⁰ This morphological difference agreed well with the variation of impact strength with filler changes (SATPGO₁ to SATPGO₂ to SATPGO₃). The SiO₂ nanoparticles attached with the GO sheets effectively prevented crack propagation, resulting rough fracture surfaces. The strong interaction between SATPGOs and epoxy matrix was confirmed by the EDX analysis where a core silica particle was interacted with the epoxy resin. In comparison to original SiO₂ nanoparticle size (about 0.007 μ m), a much larger sized SATPGOs (1.8-4.3 μ m) were recorded during fracture surface analysis. It may be attributed to the overwrapped epoxy on the silanized silica particle, as shown in Fig. 10(e, h, and k). However, there was no significant difference in fracture surface morphology between the RT-fractured and CT-fractured composites.

3.9. Microstructure analysis of the composites

TEM images of the SATPGO₁/epoxy (Fig. 11(a) and (b)), SATPGO₂/epoxy (Fig. 11 (c) and (d)) and SATPGO₃/epoxy (Fig. 11 (e) and (f)) composites are compared in Fig. 11. SATPGOs particles were dispersed in the epoxy. All the composites showed similar dispersion of nanoparticles in epoxy matrix and good interactions. However, SATPGO₂ composites showed less aggregated nanoparticles as compared to the SATPGO₁ and SATPGO₃ filled composites resulting better mechanical properties. However, in the case of the SATPGO₃/epoxy composite, an aggregated morphology was recorded. The TEM observations and mechanical property analysis demonstrated that the dispersion of the SATPGOs in the epoxy was dominated by the molecular weight of the flexible chain surface modifiers. Furthermore, the epoxy composites filled with 0.25 and 1 wt% SATPGO were also characterized using microtome TEM. Comparatively good dispersion at lower loading and a little aggregation at higher loading were observed (Fig. S5 in the supporting information).

4. Conclusions

Isocyanate group-terminated PEG flexible chains were used as cross-linkers to attach silica nanoparticles on GO sheets to prepare SATPGO. The SATPGO/epoxy composites possessed all of the advantages of the individual component materials. FT-IR, XRD, TGA, XPS, and TEM characterization were used to investigate the structural as well as morphological features of SAT, SATPGO, and SATPGO/epoxy composites with various SATPGO contents. The impact and tensile strengths, tensile modulus, and fracture toughness were measured to investigate the

mechanical properties of the SATPGO/epoxy composites. Improvement of the mechanical properties was due to the synergistic effects of the SATPGO ternary system. The fracture surface and dispersion morphology were analyzed by FE-SEM and HR-TEM analyses. The rough fracture surface was correlated with the improved mechanical properties of the composites. A load and heat were transferred easily to the silica particles and GO from the epoxy in the composites, thereby effectively improving the mechanical and thermal properties of the epoxy. In addition, the presence of PEG flexible chains interpenetrating the epoxy polymer prevented aggregation of silica nanoparticles and GO sheets in the composites.

Acknowledgement

This study was supported by the Converging Research Center Program (2013K000404) through the Ministry of Science, ICT & Future Planning and the Basic Science Research Program (NRF-2013R1A1A2011608) through the National Research Foundation (NRF) funded by the Ministry of Education of Korea.

Notes and references

^a *Applied Materials Institute for BIN Convergence (BK Plus Global Program), Dept of BIN Fusion Technology, Chonbuk National University, Jeonju, Jeonbuk, 561-756, Republic of Korea. Fax: +82 63 2702341; Tel: +82 63 270 4803*

^b *Surface Engineering and Tribology, CSIR-Central Mechanical Engineering Research Institute, Durgapur, West Bengal, 713209, India.*

^c *Center for Carbon Composites Materials, Dept of Polymer and Nano Science and Technology, Chonbuk National University, Jeonju, Jeonbuk, 561-756, Republic of Korea. Fax: +82 63 2702341; Tel: +82 63 270 4803; E-mail: jhl@jbnu.ac.kr*

* *Correspondence to: jhl@jbnu.ac.kr (J. H. Lee) and namhk99@naver.com (N. H. Kim)*

Notes and references

- D. Gautam and K. Niranjan. *Prog. Org. Coat.*, 2010, **69**, 495-503.
- P. Sudhakara, P. Kannan, K. Obireddy and A. VaradaRajulu. *J. Mater. Sci.*, 2011, **46**, 2778-2888.
- G. Yang, S. Y. Fu and J. P. Yang. *Polymer*, 2007, **48**, 302-310.
- G. Y. Nam, G. W. Yong and C. K. Sung. *Polymer*, 2004, **45**, 6953-6958.
- L. Bonnaud, J. P. Pascault, H. Sautereau, J. Q. Zhao and D. M. Jia. *Polym. Compos.*, 2004, **25**, 368-374.
- A. Saalbrink, A. Lorteije and T. Peijs. *Composites Part A*, 1998, **29**, 1243-1250.
- Saalbrink, A.; Mureau, M.; Peijs, T. *Plast. Rubber. Compos.* 2001, **30**, 213-221.
- K. C. Teng and F. C. Chang. *Polymer*, 1996, **37**, 2385-2394.
- E. M. Woo and K. L. Mao. *Polym. Compos.*, 1996, **17**, 799-805.
- C. J. Huang, S. Y. Fu, Y. H. Zhang, B. Lauke, L. F. Li and L. Ye. *Cryogenics*, 2005, **45**, 450-454.
- J. P. Yang, G. Yang, G. Xu and S. Y. Fu. *Compos. Sci. Technol.*, 2007, **67**, 2934-2940.
- J. P. Yang, Z. K. Chen, G. Yang, S. Y. Fu and L. Ye. *Polymer*, 2008, **49**, 3168-3175.
- S. Y. Fu, Q. Y. Pan, C. J. Huang, G. Yang, X. H. Liu and L. Ye. *Key. Eng. Mater.*, 2006, **312**, 211-216.
- Z. K. Chen, G. Yang, J. P. Yang, S. Y. Fu, L. Ye and Y. G. Huang. *Polymer*, 2009, **50**, 1316-1323.
- C. Mattevi, H. Kim and M. J. Chhowalla. *Mater. Chem.*, 2011, **21**, 3324-3334.
- K. S. Novoselov, A. K. Geim, S. V. Morozov, D. Jiang, M. I. Katsnelson, I. V. Grigorieva, S. V. Dubonos and A. A. Firsov. *Nature*, 2005, **438**, 197-200.
- S. V. Morozov, K. S. Novoselov, M. I. Katsnelson, F. Schedin, D. C. Elias, J. A. Jaszczak and A. K. Geim. *Phys. Rev. Lett.*, 2008, **100**, 0166021-0166024.
- X. D. Zhuang, Y. Chen, G. Liu, P. P. Li, C. X. Zhu, E. T. Kang, K. G. Neoh, B. Zhang, J. H. Zhu and Y. X. Li. *Adv. Mater.*, 2010, **22**, 1731-1740.
- Q. Wu, Y. X. Xu, Z. Y. Yao, A. R. Liu and G. Q. Shi. *ACS Nano.*, 2010, **4**, 1963-1970.
- L. Valentini, M. Cardinali, S. B. Bon, D. Bagnis, R. Verdejo, M. A. Lopez-Manchado and J. M. Kenny. *J. Mater. Chem.*, 2010, **20**, 995-1000.
- R. K. Layek, S. Samanta, A. K. Nandi. *Polymer*, 2012, **53**, 2265-2273.
- R. K. Layek, A. Kundu and A. K. Nandi. *Macromol. Mater. & Eng.*, 2013, **298**, 1166-1175.
- R. K. Layek, A. Kuila, D. P. Chatterjee and A. K. Nandi. *J. Mater. Chem. A.*, 2013, **1**, 10863-10874.
- J. H. Du, H. N. Cheng. *Macromol. Chem. Phys.*, 2012, **213**, 1060-1077.
- A. Yu, P. Ramesh, M. E. Itkis, E. Bekyarova and R. C. Haddon. *J. Phys. Chem. C.*, 2007, **111**, 7565-7569.
- D. Krishnan, F. Kim, J. Y. Luo, R. Cruz-Silva, L. J. Cote, H. D. Jang and X. J. Jang. *Nano. Today.*, 2012, **7**, 137-152.
- T. Ramanathan, A. A. Abdala, S. Stankovich, D. A. Dikin, M. Herrera-Alonso, R. D. Piner, D. H. Adamson, H. C. Schniepp, X. Chen, R. S. Ruoff, S. T. Nguyen, I. A. Aksay, R. K. Prud'Homme and L. C. Brinson. *Nat. Nanotechnol.*, 2008, **3**, 327-331.
- J. Zhu. *Nat. Nanotechnol.*, 2008, **3**, 523.
- S. Stankovich, R. D. Piner, S. T. Nguyen and R. S. Ruoff. *Carbon*, 2006, **44**, 3342-3347.
- W. Hummers and R. Offeman. *J. Am. Chem. Soc.* 1958, **80**, 1339.
- J. P. Benthem and W. T. Koiter. In: *Mechanical fracture, Methods of analysis and solutions of crack problems*. Noordhoff International Publishing: Leyden, 1975, vol. 1.
- H. K. Jeong, Y. P. Lee, M. H. Jin, E. S. Kim and J. Bae. *Chem. Phys. Lett.*, 2009, **470**, 255-258.
- S. Tama's, B. Otto and D. Imre. *Carbon*, 2005, **43**, 3186-3189.
- C. S. Shan, H. F. Yang, D. X. Han, Q. X. Zhang, A. Ivaska and L. Niu. *Langmuir*, 2009, **25**, 12030-12033.
- H. K. Jeong, Y. P. Lee, R. J. Lahaye, M. H. Park, K. H. An, I. J. Kim, C. W. Yang, C. Y. Park, R. S. Ruoff and Y. H. Lee. *J. Am. Chem. Soc.*, 2008, **130**, 1362-1366.
- G. Nallathambi, T. V. Rajendran and R. Palanivelu. *Mat. Res.*, 2011, **14**, 552-559.
- W. Cai, R. D. Piner, F. J. Stadermann, S. Park, M. A. Shaibat, Y. Ishii, D. Yang, A. Velamakanni, S. J. An, M. Stoller, J. An, D. Chen and R. S. Ruoff. *Science*, 2008, **321**, 1815-1817.
- S. Stankovich, R. D. Piner, X. Q. Chen, N. Q. Wu, S. T. Nguyen and R. S. Ruoff. *J. Mater. Chem.*, 2006, **16**, 155-158.
- C. Jill and F. M. John. *Handbook of X-ray photoelectron spectroscopy: a reference book of standard spectra for identification and interpretation of XPS data*. Eden Prairie, Minn; Physical Electronics, 1995.
- J. J. Liang, Y. Huang, L. Zhang, Y. Wang, Y. F. Ma and T. Y. Guo. *Adv. Funct. Mater.*, 2009, **19**, 2297-2302.
- D. R. Bortz, E. G. Heras and I. M. Gullon. *Macromolecules*, 2012, **45**, 238-245.
- T. Kuila, K. A. Mishra, P. Khanra, N. H. Kim, U. M. Elias and J. H. Lee. *Langmuir*, 2012, **28**, 9825-9833.
- K. N. Kudin, B. Ozbas, H. C. Schniepp, R. K. Prud'homme, I. A. Aksay and R. Car. *Nano. Lett.*, 2008, **8**, 36-41.
- C. Y. Su, Y. Xu, W. Zhang, J. Zhao, X. Tang, C. H. Tsai and L. J. Li. *Chem. Mater.*, 2009, **21**, 5674-5680.

45. A. C. Ferrari, J. C. Meyer, V. Scardaci, C. Casiraghi, M. Lazzeri, F. Mauri, S. Piscanec, D. Jiang, K. S. Jiang, S. Roth and A. K. Geim. *Phys. Rev. Lett.*, 2006, **97**, 187401-187404
- 5 46. I. Calizo, A. A. Balandin, W. Bao, F. Miao and C. N. Lau. *Nano. Lett.* 2007, **7**, 2645–2649
47. J. I. Paredes, S. Villar-Rodil, P. Solis-Fernandez, A. Martinez-Alonso and J. M. D. Tascon. *Langmuir*, 2009, **25**, 5957-5968.
- 10 48. Y. W. Zhu, M. D. Stoller, W. W. Cai, A. Velamakanni, R. D. Piner, D. Chen and R. S. Ruoff. *ACS. Nano.*, 2010, **4**, 1227-1233.
49. X. M. Jiang, T. L. Ward, Y. S. Cheng, J. W. Liu and C. J. Brinker. *Chem. Commun.*, 2010, **46**, 3019-3021
- 15 50. C. Y. Wang, L. L. Feng, H. Z. Yang, G. B. Xin, W. Li, J. Zheng, W. H. Tian and X. G. Li. *Chem. Chem. Phys.*, 2012, **14**, 13233-13238
51. C. S. Wu, Y. L. Liu, Y. C. Chiu and Y. S. Chiu. *Polym. Degrad. Stab.*, 2002, **1**, 41-48.
- 20 52. K. Apaydin, A. Laachachi, V. Ball, M. Jimenez, S. Bourbigot, V. Toniazzo and D. Ruch. *Polym. Degrad. Stab.*, 2013, **98**, 627-634.
53. X. Kong, S. S. Chakravarthula and Y. Qiao. *Int. J. Solids. Struct.*, 2006, **43**, 5969–5980.
- 25 54. Z. K. Chen, J. P. Yang, Q. Q. Ni, S. Y. Fu and Y. G. Huang. *Polymer.*, 2009, **50**, 4753-4759.
55. S. C. Kwon, T. Adachi, W. Araki and A. Yamaji. *Acta. Mater.*, 2006, **54**, 3369-3374
56. L. C. Tanga, H. Zhang, S. Sprengerb, L. Ye and Z. Zhang. *Compos. Sci. Technol.*, 2012, **72**, 558-565.
- 30 57. S. Y. Fua, X. Q. Feng, B. Lauke, Y. W. Mai. *Compos. Part: B-Eng.*, 2008, **39**, 933–961.
58. J. J. Park, K. G. Yoon and J. Y. Lee. *Trans. Electr. Electron. Mater.*, 2011, **12**, 98-101.
- 35 59. X. F. Yi, A. K. Mishraa, N. H. Kim, B. C. Ku and J. H. Lee. *Compos. Part. A: Appl. Sci. Manufac.*, 2013, **49**, 58–67.
60. K. Wang, L. Chen, J. S. Wu, M. L. Toh, C. B. He, A. F. Yee. *Macromolecules*, 2005, **38**, 788-800.

Fig. 8 Fracture toughness of pure epoxy, SATPGO/epoxy composites with various filler content.

Fig. 9 (a) Storage modulus and (b) $\tan \delta$ versus temperature curves of pure epoxy and SATPGO₁ (0.5 wt%)/epoxy, SATPGO₂ (0.5 wt%)/epoxy and SATPGO₃ (0.5 wt%)/epoxy.

Fig. 10 E-SEM images of impact fractured surface of (a, b) pure epoxy at RT and CT; (c, d) SATPGO₁ (0.5 wt%) /epoxy at RT and CT; (e) EDX of SATPGO₁ (0.5 wt%) /epoxy, (f, g) SATPGO₂ (0.5 wt%) /epoxy at RT and CT; (h) EDX of SATPGO₂ (0.5 wt%) /epoxy, (i, j) SATPGO₃ (0.5 wt%) /epoxy at RT and CT, (k) EDX of SATPGO₃ (0.5 wt%) /epoxy.

Fig. 11 HR-TEM images of (a and b) SATPGO₁ (0.5 wt%)/epoxy, (c and d) SATPGO₂ (0.5 wt%)/epoxy, (e and f) SATPGO₃ (0.5 wt%)/epoxy.

40 Figure Captions

Fig. 1 FT-IR spectra of SiO₂, SA, SAT, SATPGO₂, and GO.

Fig. 2 XRD plots of SiO₂, SATPGO₂, GO, and graphite. The inset of Fig. 2 shows the XRD plots of SiO₂, SATPGO₂, GO, and graphite at low angle.

45 **Fig. 3** XPS survey curves of (a) GO, (b) SATPGO₂, (c) C1s of GO, (d) C1s of SATPGO₂, (e) Si2p of SATPGO₂, (f) N1s of SATPGO₂.

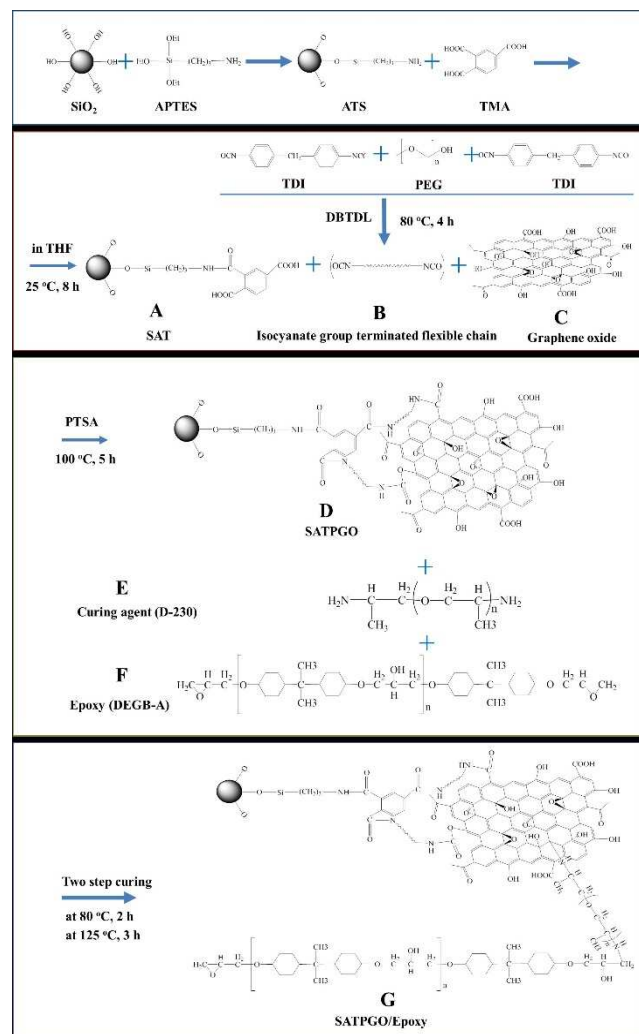
Fig. 4 Transmission electron micrographs of (a) GO, (b) SATPGO₂, and (c) SAED patterns of (d) SATPGO₂.

50 **Fig. 5** Raman spectra of GO, SATPGO₁, SATPGO₂, SATPGO₃, SATPGO₁/epoxy (0.5 wt%), SATPGO₂/epoxy (0.5 wt%), and SATPGO₃/epoxy (0.5 wt%).

Fig. 6 TGA curves of (a) SiO₂, SA, SAT, GO, SATPGO₁, SATPGO₂, SATPGO₃, pure epoxy, SATPGO₁ (0.5 wt%)/epoxy, SATPGO₂ (0.5 wt%)/epoxy, and SATPGO₃ (0.5 wt%)/epoxy in N₂, (b) pure epoxy, SATPGO₁ (0.5 wt%)/epoxy, SATPGO₂ (0.5 wt%)/epoxy, and SATPGO₃ (0.5 wt%)/epoxy in air.

Fig. 7 (a) Tensile strength, (b) tensile modulus and (c) Impact strength of SATPGO/epoxy composites with various filler content at RT and CT.

Figures



Scheme. 1

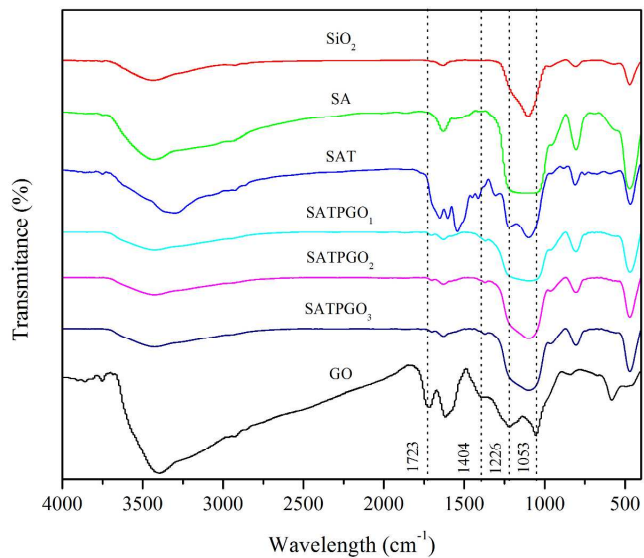


Fig. 1

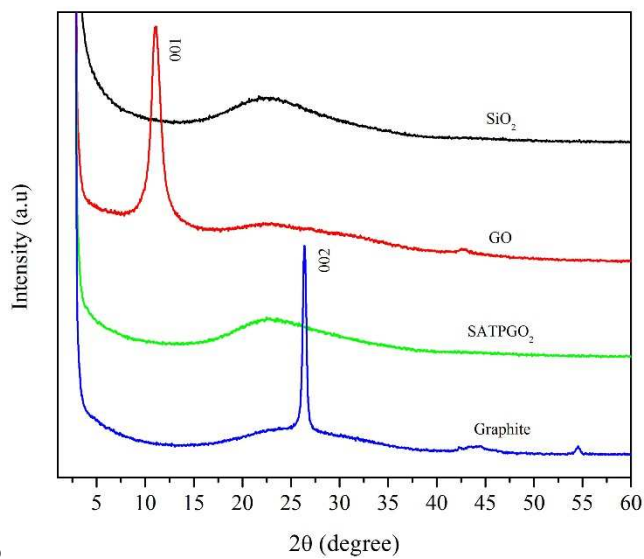


Fig. 2

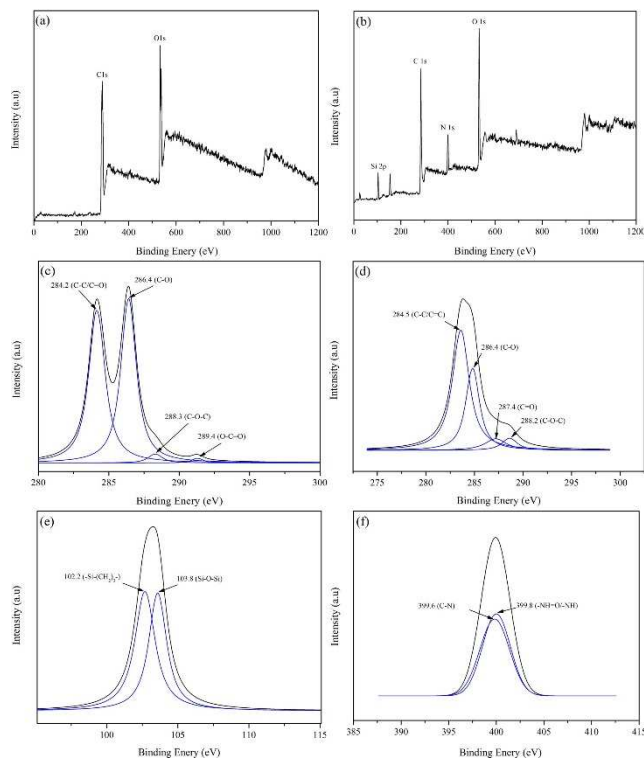


Fig. 3

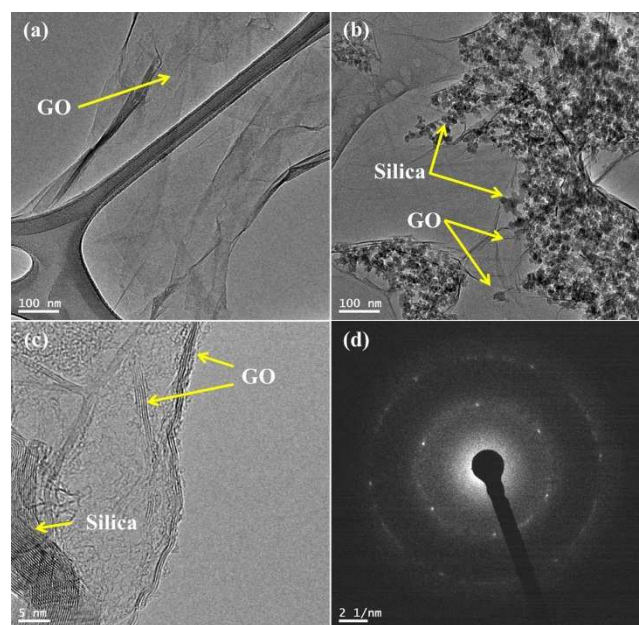


Fig. 4

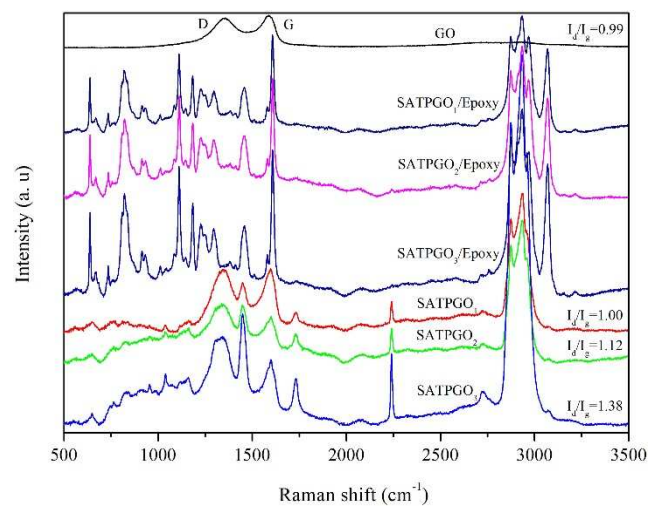


Fig. 5

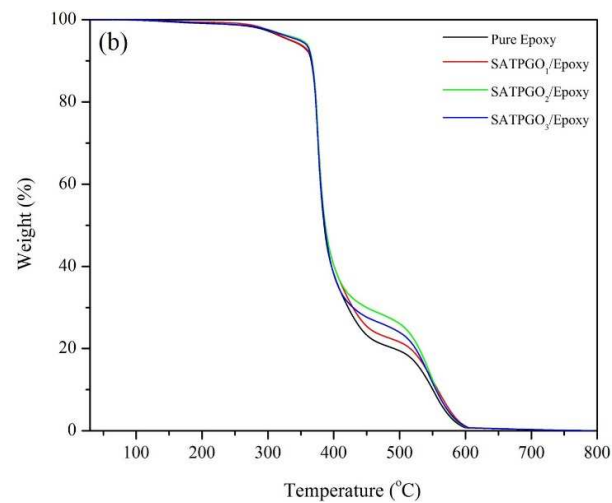
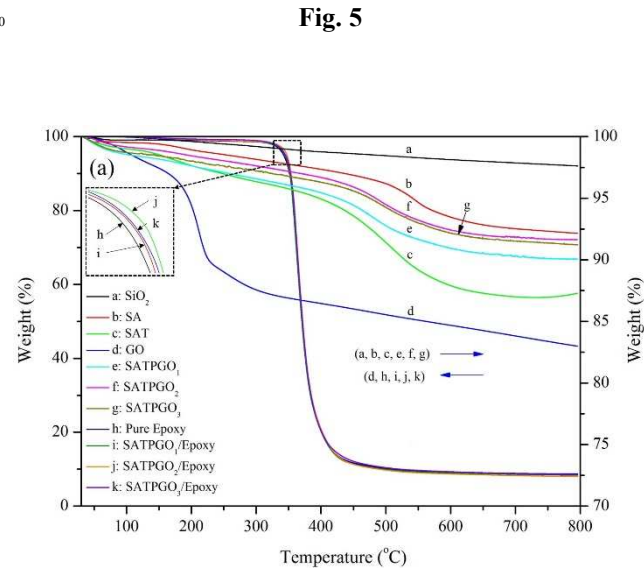


Fig. 6

5

15

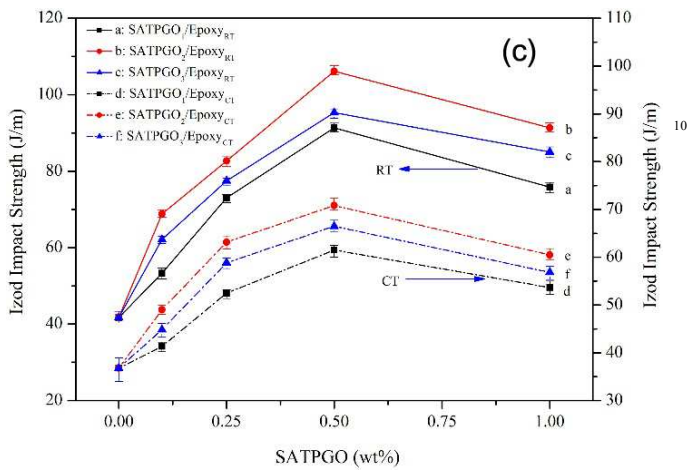
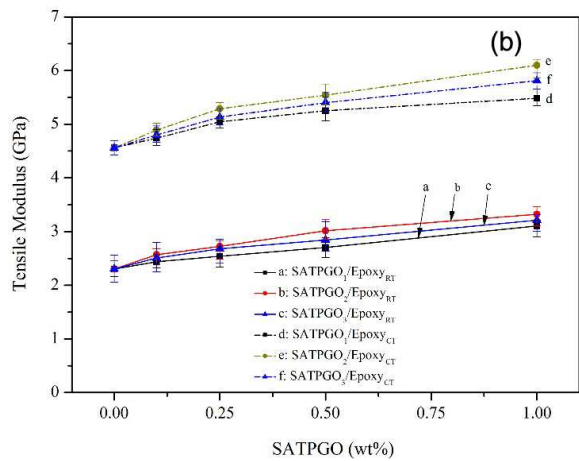
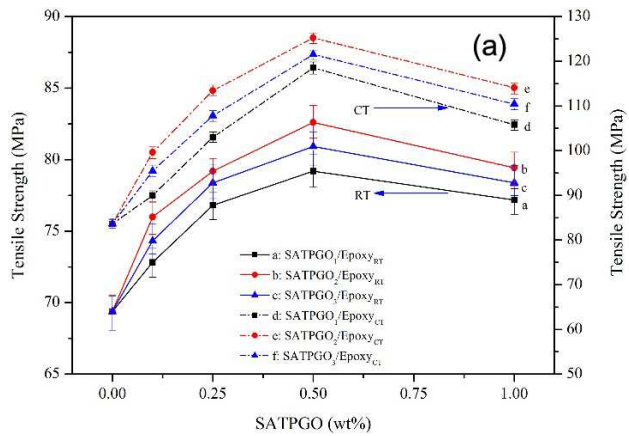


Fig. 7

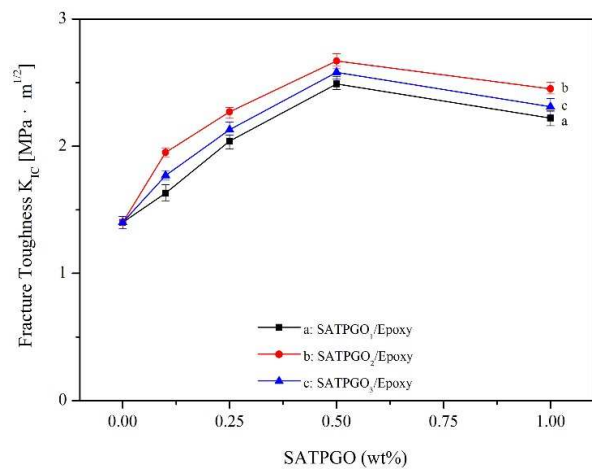


Fig. 8

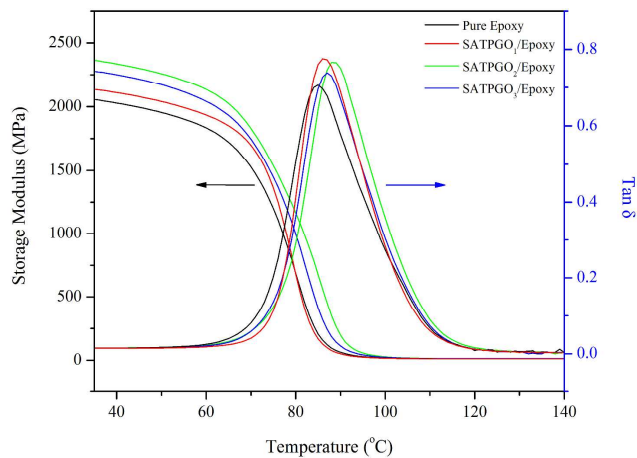


Fig. 9

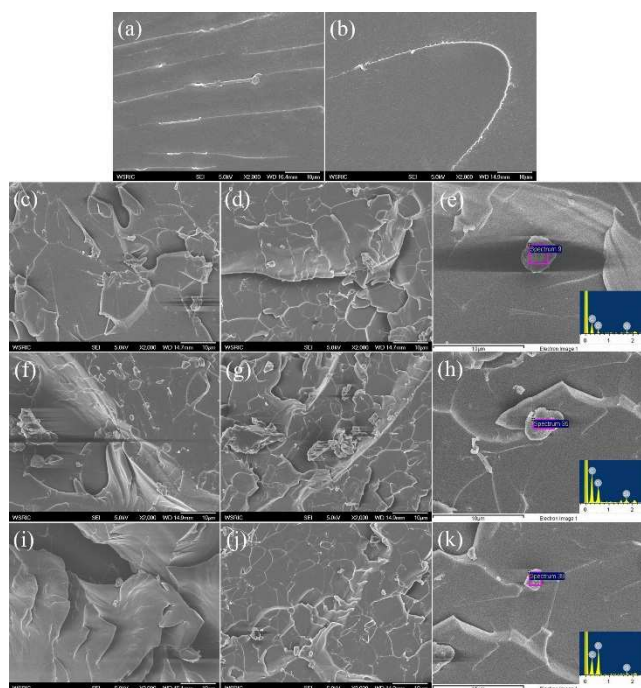


Fig. 10

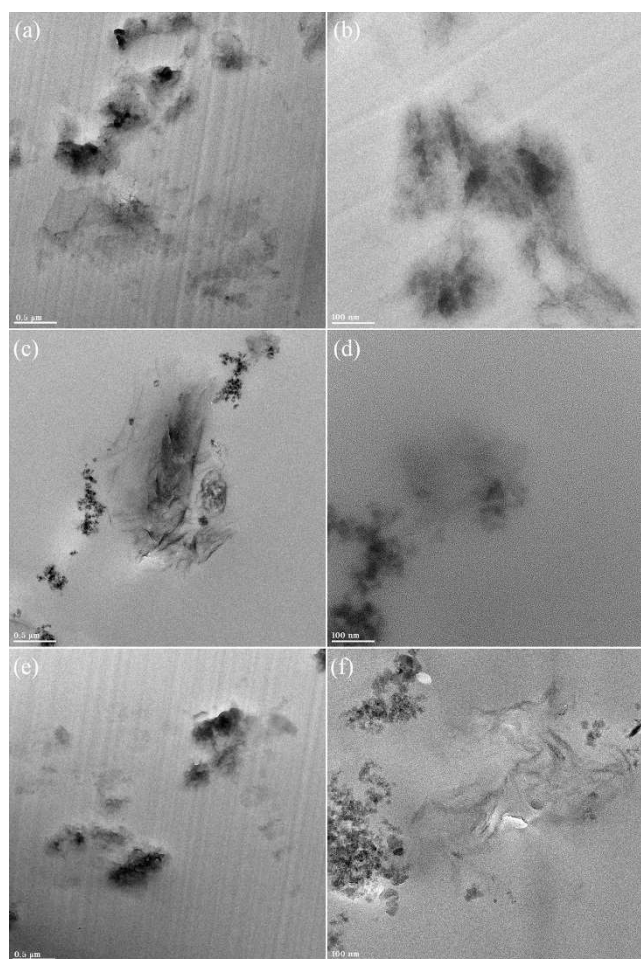


Fig. 11

5

Table of Content

Surface modified silica nanoparticles attached graphene oxide using isocyanate terminated flexible chains were used for toughening epoxy.

